



ORIGINAL RESEARCH

Resting-state functional connectivity modulates the BOLD activation induced by nucleus accumbens stimulation in the swine brain

Shinho Cho^{1,2}  | Jan T. Hachmann^{1,3} | Irena Balzekas⁴ | Myung-Ho In^{1,5} |
Lindsey G. Andres-Beck⁶ | Kendall H. Lee^{1,6} | Hoon-Ki Min^{1,5,6} | Hang Joon Jo^{1,4,5,7} 

¹Department of Neurologic Surgery, Mayo Clinic, Rochester, MN, USA

²Center for Magnetic Resonance Research, Department of Radiology, University of Minnesota at Twin Cities, Minneapolis, MN, USA

³Department of Neurologic Surgery, Virginia Commonwealth University Health System, Richmond, VA, USA

⁴Department of Neurology, Mayo Clinic, Rochester, MN, USA

⁵Department of Radiology, Mayo Clinic, Rochester, MN, USA

⁶Department of Biomedical Engineering and Physiology, Mayo Clinic, Rochester, MN, USA

⁷Department of Physiology, College of Medicine, Hanyang University, Seoul, South Korea

Correspondence

Hang Joon Jo, Department of Physiology, College of Medicine, Hanyang University, Seoul, South Korea.

Email: hangjoonjo@hanyang.ac.kr

Funding information

Hanyang University, Grant/Award Number: HY-2019; National Institutes of Health, Grant/Award Number: NIH C06 RR018898 and NIH R01 NS70872; The Grainger Foundation

Abstract

Introduction: While the clinical efficacy of deep brain stimulation (DBS) the treatment of motor-related symptoms is well established, the mechanism of action of the resulting cognitive and behavioral effects has been elusive.

Methods: By combining functional magnetic resonance imaging (fMRI) and DBS, we investigated the pattern of blood-oxygenation-level-dependent (BOLD) signal changes induced by stimulating the nucleus accumbens in a large animal model.

Results: We found that diffused BOLD activation across multiple functional networks, including the prefrontal, limbic, and thalamic regions during the stimulation, resulted in a significant change in inter-regional functional connectivity. More importantly, the magnitude of the modulation was closely related to the strength of the inter-regional resting-state functional connectivity.

Conclusions: Nucleus accumbens stimulation affects the functional activity in networks that underlie cognition and behavior. Our study provides an insight into the nature of the functional connectivity, which mediates activation effect via brain networks.

KEYWORDS

blood-oxygenation-level-dependent hemodynamic response, deep brain stimulation, functional connectivity change, functional magnetic resonance imaging, network effect, nucleus accumbens, resting-state functional connectivity

1 | INTRODUCTION

While deep brain stimulation (DBS) is an established therapy for the treatment of essential tremors (Benabid et al., 1991), Parkinson's disease (PD) (Benabid, 2003; Deep-Brain Stimulation for Parkinson's Disease Study Group, 2001), and dystonia (Coubes

et al., 2004), the recent use of DBS has expanded into the realm of neuropsychiatric disorders, that is, obsessive-compulsive disorder (OCD) (Greenberg et al., 2010, 2006; Mallet et al., 2008), treatment-refractory depression (TRD) (Denys et al., 2010; Mayberg et al., 2005; Schlaepfer et al., 2008), addiction (Kuhn et al., 2009, 2007), and Tourette's syndrome (TS) (Houeto et al., 2005; Servello,

This is an open access article under the terms of the Creative Commons Attribution License, which permits use, distribution and reproduction in any medium, provided the original work is properly cited.

© 2019 The Authors. *Brain and Behavior* published by Wiley Periodicals, Inc.

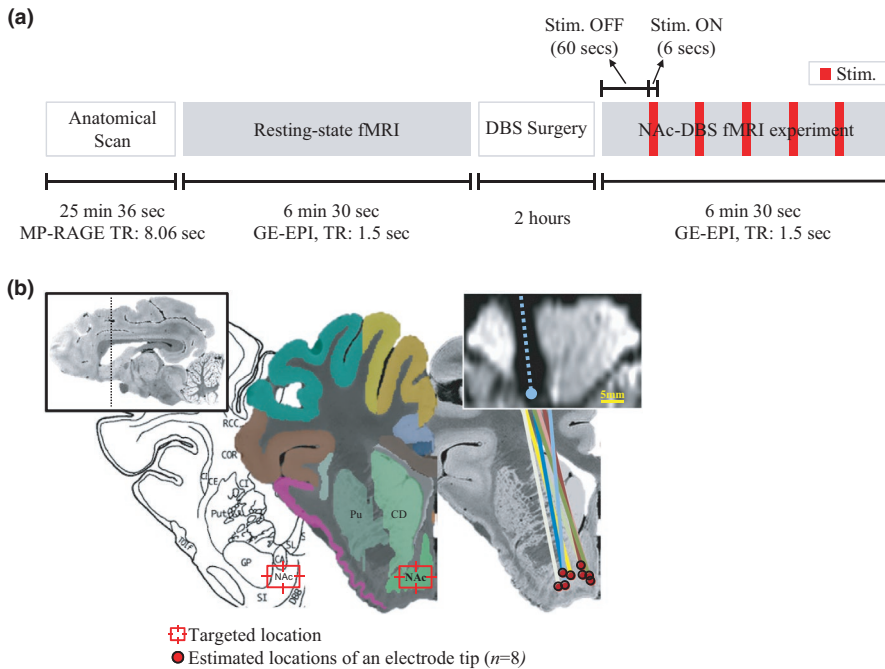


FIGURE 1 (a) Schematic diagram depicting the experimental procedure and (b) the placement of electrode in the placement of subjects on the pig brain atlas (Saikali et al., 2010). The red dots and colored lines indicate the estimated position of an individual electrode tip and body, respectively ($n = 8$). The postsurgical echo-planar image in a coronal view is shown on the top right (a single subject), wherein the signal dropout induced by electrode body. See for the abbreviations in Appendix A

Porta, Sassi, Brambilla, & Robertson, 2008). Cumulative results suggest that abnormal functional coupling between brain regions may be associated with neuropsychiatric diseases, that is, the cortico-striato-thalamo-cortical (CSTC) circuit and the orbitofrontal cortex (OFC) (Greenberg et al., 2010, 2006; Rauch et al., 1994; Volkow, Fowler, Wang, Swanson, & Telang, 2007). However, the issue of how DBS alters functional coupling in potentially disease-related brain networks and the nature of the biological mechanism that supports the DBS effect remain unclear (McIntyre & Hahn, 2010; Vitek, 2002).

NAc-DBS has a demonstrated clinical efficacy, although the effects are serendipitous, and the mechanism of action is elusive, for alleviating the symptoms of comorbid depression and obsessive-compulsive mental symptoms (Bewernick et al., 2010; Hamani et al., 2014; Nuttin, Cosyns, Demeulemeester, Gybels, & Meyerson, 1999; Rasmussen, Greenberg, Mindus, Friehs, & Noren, 2000). Since DBS action is thought to alter functional coupling and regularize abnormal brain signals, previous studies have suggested that stimulating NAc influenced neural signaling between the ventral striatum and the prefrontal cortex (Figuee et al., 2013), resulted in attenuating pathological hyperactivity (Baxter et al., 1992; McCracken & Grace, 2007; Rauch et al., 1994; Swedo, Rapoport, Leonard, Lenane, & Cheslow, 1989). However, it has recently been revealed that the DBS effect, while not specifically stimulating the NAc, appeared as widespread BOLD hemodynamic changes across the global brain, that is, throughout cognitive, limbic, and sensorimotor networks, as evidenced by functional imaging (Gibson et al., 2016; Knight et al., 2013; Krack, Hariz, Baunez, Guridi, & Obeso, 2010).

It is clear that NAc-DBS induced its own BOLD activation pattern, as stimulating targets have their own unique, target-specific

modulation effects (Gibson et al., 2016; Knight et al., 2013; Krack et al., 2010; Min et al., 2012; Paek et al., 2015; Settell et al., 2017). However, it is unclear which specific neurobiological mechanism mediates broadly distributed BOLD activation patterns. Since BOLD activation can be found across anatomically heterogeneous regions that may not be directly connected to the stimulation site, an anatomical connection would not likely be the exclusive mechanism for delivering the DBS effect, albeit some anatomical connections have been found in DBS-activated regions from diffusion tensor imaging (DTI) and fiber tracing studies in animal models (Britt et al., 2012; Leh, Ptito, Chakravarty, & Strafella, 2007; Lehericy et al., 2004).

We investigated the pattern and extent of BOLD activation and changes in functional connectivity between activated brain regions after high frequency stimulation in a healthy pig model. In particular, we observed changes in inter-regional functional connectivity (rsFC), focused on brain regions that evoked a significant BOLD response to NAc-DBS, including executive, limbic, thalamic, and sensorimotor networks. Furthermore, we also conducted rsFC mapping (Biswal, Zerrin Yetkin, Haughton, & Hyde, 1995; Fox, Halko, Eldaief, & Pascual-Leone, 2012) for each subject prior to the DBS implantation surgery in order to collect information on the relationship between the strength of rsFC and BOLD activation, as a potential action mechanism of DBS, which has been overlooked in previous DBS-fMRI studies (Gibson et al., 2016; Min et al., 2012; Paek et al., 2015; Settell et al., 2017). The use of a large animal model in our study is presumably more representative of the human brain anatomy (Van Gompel et al., 2011) than small animal models (Albaugh et al., 2016), and therefore, our findings should be assumed to be general in nature, in terms of understanding the therapeutic effects of human DBS.

2 | MATERIALS AND METHODS

2.1 | Animal model and preparation

Eight male domestic pigs (*sus scrofa domesticus*, 8–12 months old, 25–30 kg) were initially sedated with an intramuscular injection of a ketamine (10–20 mg/kg) and xylazine (2.5 mg/kg) cocktail. Each animal was then orally intubated and mechanically ventilated by a medical-grade pressure-driven mechanical ventilator (respiration cycle: 12 per min) with a 7:3 N₂O:O₂ medical gas mixture. Anesthesia was maintained with a constant gas flow of isoflurane (concentration: 1.2%–1.4% for imaging experiment and 2% for DBS surgery). Animal physiology was measured with a MR compatible pulse oximetry and capnography sensor (Nonin Medical Inc) and maintained at normal conditions (heart rate: ~120 bpm, SpO₂: 98%–100%, and end-tidal CO₂: 3.5%–4%). The rectal temperature (PhysiTemp Instrument) was monitored (37 ± 1°C) and maintained using a heated circulating water blanket. Animal surgical procedures and experimental protocol were approved by the Institutional Animal Care and Use Committee of the Mayo Clinic.

2.2 | Experimental outline

Figure 1a outlines the experimental timeline. After initial sedation and intubation, the animal was delivered to a scanner for imaging for an individual anatomical scan (25 min 36 s). The anatomical scan was followed by a resting-state functional MRI (6 min 30 s). After resting-state functional imaging, electrode implantation surgery was followed (2 hr) and the DBS-fMRI experiment was carried out (6 min 30 s).

2.2.1 | Anatomical imaging

High-resolution anatomical T1-weighted images were obtained with a GE 3-Tesla Signa Excite scanner using a custom-built 8-channel surface-type radio frequency (RF) coil with following imaging protocols: A 3D magnetization prepared radio frequency pulses and rapid gradient echo (MP-RAGE) sequence, TR/TE = 8.06/3.3 ms, inversion time = 1,000 ms, flip angle = 8°, slice thickness = 0.8 mm, matrix size = 300 × 300 × 108, field of view (FOV) = 240 × 240 × 87 mm³, average number = 2, and total scan time = 25 min 36 s.

2.2.2 | Resting-state functional imaging

After anatomical imaging, resting-state functional imaging was conducted with the following imaging protocols: gradient echo echo-planar imaging (GE-EPI), TR/TE = 1,500/40 ms, slice thickness = 2.4 mm, 19 slices, field of view (FOV) = 160 × 160 mm², matrix size = 96 × 96, voxel resolution = 1.67 × 1.67 × 2.4 mm³, and total scan time = 6 min 30 s.

2.2.3 | DBS electrode implantation

A quadripolar DBS electrode (Model 3389; Medtronic Inc.) was implanted targeting to NAc of the left hemisphere (Knight et al., 2013;

Min et al., 2012). The coordinates (arc, collar, and depth) on a stereotactic frame (Leksell; Elekta Co) were determined by COMPASS planning software (COMPASS International Innovations) based on NAc location identified from individual subject's anatomical brain images (Knight et al., 2013) (Figure 1b). Microdrive (Alpha Omega Co.) was used to guide the implantation of a DBS lead. All of these systems can minimize the displacement of an electrode from a targeted position (<1 mm), as shown in our previous phantom tests (Min et al., 2014).

2.2.4 | DBS stimulation parameters and DBS-fMRI acquisition

Following DBS surgery, each animal underwent functional imaging with simultaneous NAc stimulation. Each stimulation block consisted of a 6-s stimulation train followed by a 60-s off period stimulation (Figure 1a). The block was repeated five times per scan with the initial baseline period. The total time per scan was 6 min and 30 s. The imaging parameters were the same with those in the resting-state scan were used.

The stimulation parameters were as follows: biphasic and bipolar pulse, voltage = 5 V, pulse frequency = 130 Hz, and pulse duration = 100 μs. These parameters were selected based on results from our previous study wherein we found a robust and reproducible BOLD activation in multiple trials across different subjects (Knight et al., 2013; Min et al., 2012; Paek et al., 2015; Settell et al., 2017).

2.3 | fMRI data preprocessing

Resting-state and DBS-fMRI data were processed using the AFNI software (Cox, 1996). Animal physiological data were collected to remove image artifacts. Respiration cycle and cardiac pulsations were measured by a respiratory bellows positioned at the level of the abdomen and a pulse oximetry placed on the animal's left ankle. Data were recorded through the scanner (3T Signa Excite MRI scanner; GE Medical Systems), and timing was synchronized with scan start and stop of EPI sequence. To remove physiological artifacts, regressors for modeling respiration and cardiac activity, and respiration volume per time (RVT) were created and subtracted out from individual BOLD time course in slice by slice, according to the pipe line of the RETROICOR + RVT (Birn, Diamond, Smith, & Bandettini, 2006).

Spike removal, slice-timing correction, and within-subject motion correction with six parameters (three translations and three rotations of x-, y-, and z-axis) were applied. Individual subject's anatomical and functional images were coregistered to the pig brain atlas using a 9-parameter linear registration (3-translation, 3-rotation, and 3-scaling) with the cost function of the Hellinger distance (Mallet et al., 2008), and the alignment of coregistration was then visually checked each time. Prior to statistical analysis, spatial smoothing was applied using 3-mm full-width-half-maximum (FWHM) isotropic Gaussian kernel. A temporal filter was not used in this study, because the physiological artifacts were regressed out, and temporal filtering could influence the temporal

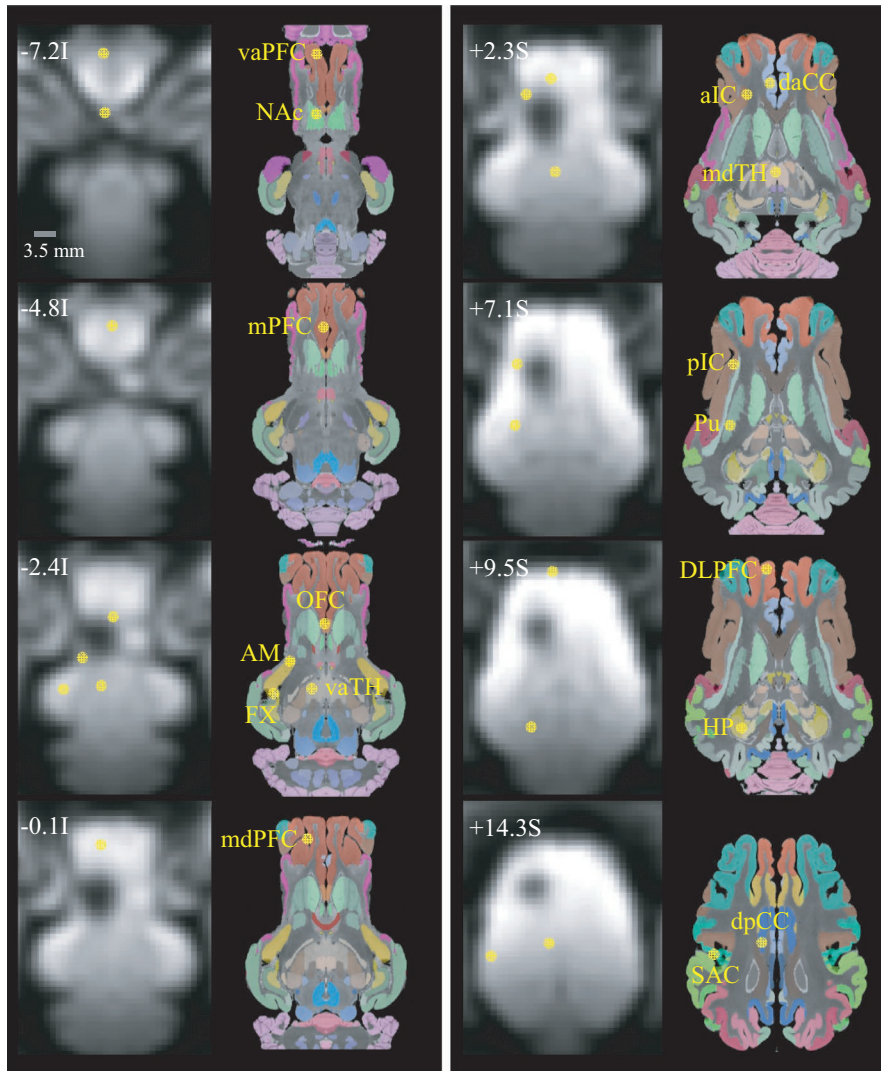


FIGURE 2 Region of interests (ROIs). The location and perimeter of region of interests (ROIs) are shown as yellow circles on postsurgical EPI images. Each region consisted of voxels in a radius within 1.7 mm from the location of the peak BOLD activation. The anatomical labels were presented together for reference. See for the abbreviations in Appendix A

synchronization between imaging and stimulation onset (Davey, Grayden, Egan, & Johnston, 2013).

2.4 | DBS-fMRI BOLD activation map

The general linear model (GLM) analysis was adopted to detect stimulation-induced BOLD activation and measure the amplitude of signal change. An individual analysis was carried out first, and a group-level ($n = 8$) statistical analysis was then performed (3dDeconvolve and 3dttest, AFNI). In the group-level analysis, significant BOLD activation was detected with the threshold, set as $p < .05$ ($n = 8$, $t > 3.49$, false discovery rate [FDR] corrected). The coordinates, t -scores, and percent signal changes were summarized. The activation map was created with different color encoding based on the percent change in a signal and overlaid on the pig brain atlas in three view planes (axial, coronal, and sagittal).

2.5 | Region of interest generation

Figure 2 shows the locations of the region of interests (ROIs) used in this study (see Appendix A for list of ROI abbreviations). The

location of ROIs was determined based on a group-level BOLD activation map, wherein significant stimulation-induced activation was observed.

BOLD time courses for each ROI were generated. We first created a sphere mask (radius = 1.7 mm) and applied it on the center location of each ROI. We then extracted all time courses within the mask and averaged them individually, and generated the group-averaged ROI time courses ($n = 8$).

2.6 | Functional connectivity analysis

Functional connectivity (FC) analyses were conducted on data obtained during resting, stimulation, and poststimulation state. To calculate the resting-state FC, the Pearson correlation coefficient (CC) was calculated between ROI time courses. For estimating stimulation and poststimulation-state FC calculations, individual time courses were divided into two time periods: the first 30-s data points after stimulation onset (stimulation state FC) and the later 30-s data until the beginning of the following stimulation block (poststimulation state FC). For each subject, coefficient matrices were averaged across blocks, generating a single stimulation- or

poststimulation-state matrix. Finally, individual subject's CC matrices were normalized by Fisher's Z-transformation and averaged into a group-level CC matrix ($n = 8$). To detect significant FC during resting state, one-sample t test was applied. To detect the significant change of FC, two-sample t test was used between resting- and poststimulation-state CC matrix.

2.7 | The relationship between resting-state functional connectivity and the BOLD response

Pearson's CC (r) and slope of linear regression (s) were estimated between the resting-state functional connectivity (rsFC) of a given ROI to the NAc and the BOLD response of the ROI. In the voxel-wise analysis, the same calculation was conducted: the sphere mask (radius = 1.7 mm) was applied to individual voxel in functional networks, and a voxel-wise averaged time course was obtained. Then, statistics (r and s) between rsFC-to-NAc and BOLD response of a given voxel were estimated. Data points were categorized into five functional networks to plot separately.

The correlation and regression analyses were also applied between inter-ROI rsFC and inter-ROI FC change in poststimulation state. The same sort of analysis was applied to analyze the relationship between co-activation of ROIs and inter-ROI FC change in poststimulation state. In those analyses, the absolute CC value was considered.

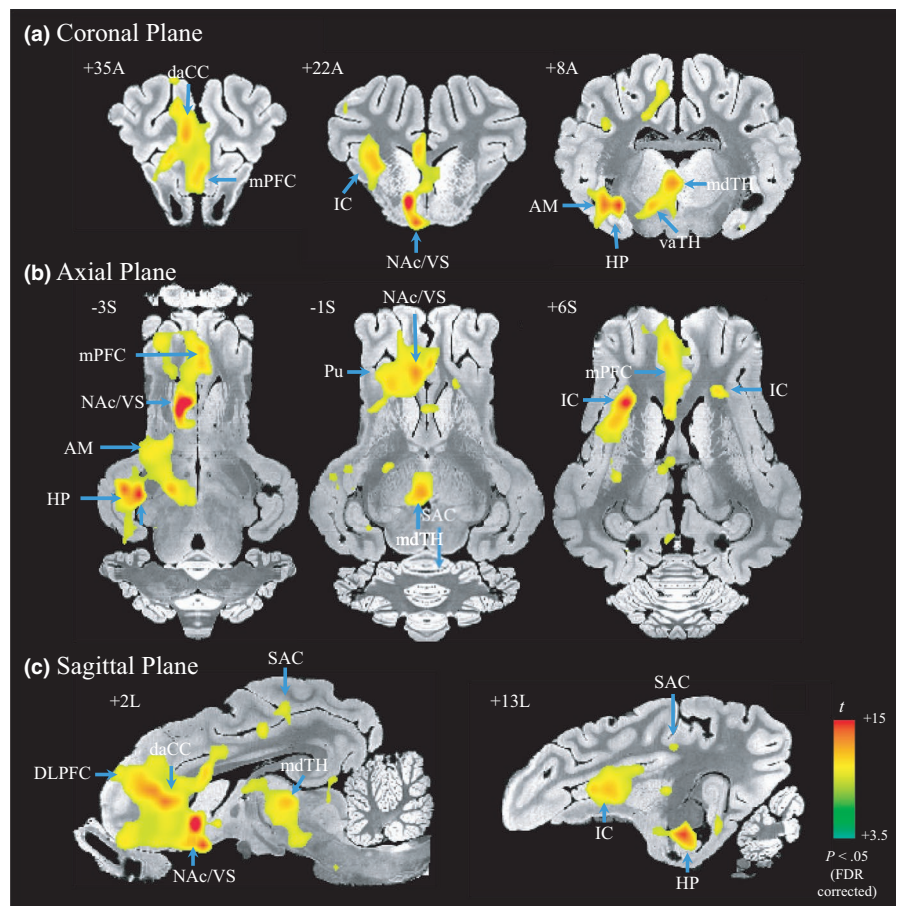
2.8 | Postsurgical evaluation of DBS electrode placement

The placement of the lead and location of electrode tip was examined by reconstructing an electrode-induced image artifact on individual EPI image volumes (Horn & Kühn, 2015). Intensity thresholding was applied to the axial plane of a single EPI image slice. The signal dropout region induced by the image artifact was isolated, and centroids of the region were marked along with the slice direction. By interpolating those marks, the lead placement could be reconstructed on individual anatomical image volumes. The location of the electrode tip with contacts 0 and 1 was then estimated and mapped on the pig brain atlas (Figure 1b).

2.9 | Comparison of EPI signal intensity in stimulation on and off periods

Echo-planar imaging image volumes, obtained during stimulation on and off periods, were averaged across blocks. Voxel-wise signal intensity was extracted within and adjacent area of the signal dropout region. Data points of stimulation on and off period were plotted separately with spatial distance. The statistical analysis (two-sample t test) between the signal intensities of stimulation on and off blocks was conducted to detect the significance of signal difference in conditions.

FIGURE 3 Group-level BOLD activation map of a 130 hz NAc-DBS ($n = 8$; $t > 3.5$; $p < .05$, false discovery rate [FDR] corrected). Activated regions are shown in (a) coronal, (b) axial, and (c) sagittal views on the pig brain atlas (Saikali et al., 2010), and the t -scores for activation are denoted by colors. NAc-DBS induced BOLD activation in multiple cortical and subcortical brain regions. Note that DBS electrodes were implanted in the left hemisphere for all subjects. For abbreviations, see Appendix A



3 | RESULTS

3.1 | BOLD activation induced by NAc-DBS

NAc-DBS evoked significant BOLD activation in multiple cortical and subcortical brain regions, but was limited to the ipsilateral hemisphere (Figure 3). The highest amplitude of evoked BOLD activation was found in the ipsilateral NAc (signal change: $1.27 \pm 0.19\%$, beta coefficient: 1.6, $t = 12.11$, $p < .05$, false discovery rate [FDR] corrected), indicating the current spread near the DBS electrode tip likely evoked a direct neuromodulatory effect (McIntyre, Mori, Sherman, Thakor, & Vitek, 2004). However, it must be noted that BOLD activation was also evident beyond the stimulation locus, that is, prefrontal, cingulate, insular, and sensorimotor cortices ($p < .05$,

FDR corrected) (see Table 1 for the summary of activated clusters). Thus, the results show NAc-DBS induced both local and distal modulatory effects across multiple functional networks including executive, limbic, thalamic, and sensorimotor networks. Interestingly, such effect was primarily lateralized to the left hemisphere, ipsilateral to the DBS electrode (Figure 3b). Only a few regions in the contralateral hemisphere (pIC, CD, Pu, and premotor cortex) showed significant BOLD activation ($p < .05$, FDR corrected), demonstrating that the DBS effect may be unilateral.

Figure 4 shows group-averaged ROI time courses by individual region. The DBS evoked BOLD response was characterized by an initial negative induction (5 ± 3 s) followed by peaks (25 ± 5 s), which is consistent with previously published hemodynamic responses to visual and sensory stimulation (Ogawa et al., 1992, 1993).

TABLE 1 The summary of BOLD activation clusters

Regions	MNI coordinate [mm]			t	GLM Beta	Max % change (± 1 SEM)
	X	Y	Z			
Ipsilateral stimulation hemisphere (left)						
Executive/prefrontal						
Dorsal lateral prefrontal cortex (DLPFC)	5.10	-35.27	10.45	5.61	1.37	0.76 ± 0.20
Medial prefrontal cortex (mPFC)	0.90	-34.97	-4.85	7.66	1.14	0.79 ± 0.14
Medial dorsal prefrontal cortex (mdPFC)	5.10	-35.27	0.25	7.40	1.60	1.06 ± 0.21
Orbitofrontal cortex (OFC)	0.90	-23.27	-2.45	6.81	0.91	0.79 ± 0.42
Ventral anterior prefrontal cortex (vaPFC)	2.40	-38.27	-6.95	6.36	1.05	0.68 ± 0.15
Executive/insular						
Anterior insular cortex (aIC)	7.20	-26.58	2.05	7.77	1.45	1.05 ± 0.14
Posterior insular cortex (pIC)	10.80	-23.27	7.15	13.64	1.20	1.01 ± 0.14
Limbic/basal ganglia						
Amygdala (AM)	10.80	-12.78	-2.45	6.58	1.87	1.29 ± 0.15
Fornix (FX)	15.90	-4.38	-2.45	11.78	0.59	0.54 ± 0.12
Nucleus accumbens (NAc)	2.40	-21.47	-7.25	12.11	1.63	1.27 ± 0.19
Putamen (Pu)	12.60	-6.48	6.55	4.99	0.47	0.44 ± 0.12
Hippocampus (HP)	10.90	7.50	9.60	5.90	0.31	0.36 ± 0.12
Dorsal anterior cingulate cortex (daCC)	2.40	-29.88	2.35	10.20	1.43	1.06 ± 0.18
Dorsal posterior cingulate cortex (dpCC)	4.20	-6.48	14.65	7.61	0.23	0.27 ± 0.12
Sensorimotor						
Somatosensory association cortex (SAC)	15.30	-0.48	21.25	4.75	0.54	0.68 ± 0.08
Thalamus						
Medial dorsal thalamus (mdTH)	0.60	-4.07	2.35	9.73	0.84	0.83 ± 0.12
Ventral anterior thalamus (vaTH)	5.70	-4.37	-2.45	9.13	0.46	0.42 ± 0.12
Contralateral hemisphere (right)						
Executive/insular						
Posterior insular cortex (pIC)	-9.50	-24.80	7.20	6.20	0.25	0.21 ± 0.05
Limbic/basal ganglia						
Caudate (CD)	-4.50	-17.87	-2.45	4.67	0.36	0.23 ± 0.09
Putamen (PU)	-6.10	-9.50	9.60	5.98	0.35	0.33 ± 0.05
Sensorimotor						
Premotor	-2.70	-19.70	16.80	5.05	0.34	0.31 ± 0.07

3.2 | Resting-state functional connectivity

In the resting-state functional imaging results, mdPFC, daCC, aIC, pIC, OFC, and NAc showed significantly coherent inter-regional BOLD activity (group-average $r = 0.21\text{--}0.65$, $n = 8$, $t > 2.37$, $p < .05$, FDR corrected) (Figure 5a), indicating the presence of functional connectivity among those regions. In particular, NAc, of these ROIs, showed strong connectivity to the mdPFC, OFC, insula, and daCC, consistent with previously reported findings in animal (Morgane, Galler, & Mokler, 2005) and human studies (Cauda et al., 2011; Di Martino et al., 2008; Knutson, Adams, Fong, & Hommer, 2001). Additionally, daCC showed a broad connectivity to many other brain regions including the prefrontal regions, aIC, and NAc as shown in other resting-state FC studies (Cauda et al., 2011; Greicius, Krasnow, Reiss, & Menon, 2003). Our results show that functional coupling could be observed between anatomically separate brain regions under conditions of isoflurane anesthesia.

3.3 | Co-activation of ROIs during stimulation

NAc-DBS evoked temporally synchronized hemodynamic responses in ROIs of the ipsilateral prefrontal cortex ($r > 0.3$, $n = 8$, $t > 2.37$, $p < .05$) (Figure 5b). Importantly, it should be noted that co-activation was found between regions, wherein their anatomical connections are less clear, such as those between the prefrontal cortex and the thalamus. These results support the fact that distal effect of NAc-DBS cannot be fully explained by a direct inter-regional anatomical connection alone, albeit the co-activations in anatomically adjacent regions would not be surprising, that is, regions within limbic system or prefrontal cortex.

3.4 | Relationship between resting-state functional connectivity to NAc and amplitude of BOLD activation

We found that a significant positive relationship exists between the rsFC-to-NAc of individual ROIs and their BOLD response ($r = 0.52$, $p < .01$) (Table 1 and Figure 6a). The stronger rsFC to the stimulation locus (NAc) that was presented, the higher was the BOLD response. The relationship between the rsFC and BOLD response, however, was observed, not only in regions of activation above the statistical threshold ($p < .05$). Rather, the voxel-wise analysis for expanded region of interests further revealed that BOLD response was correlated with the connectivity, that is, voxels in the bilateral executive and limbic networks ($r = 0.16\text{--}0.43$, $s = 0.17\text{--}1.42$, $p < .01$) (Figure 6b,c). Additionally, the relationship in the thalamic network was opposite from each other across the two hemispheres ($r = 0.38$ in the ipsilateral hemisphere, and $r = -0.23$ in the contralateral hemisphere) and no significant relationship was found in both sensorimotor networks. The results of both ROI and voxel-wise analysis support the conclusion that functional connectivity, originated from the stimulation locus, may mediate the distal BOLD activation in remote regions.

3.5 | The change in pair-wise FC connectivity during poststimulation state

Significant decreases in FC ($p < .05$) were found between many regions in the poststimulation period, that is, daCC, dpCC, pIC, DLPFC, and vaTH (Figures 7 and 8); however, some others were enhanced after stimulation, that is, the pairs of VS-mdPFC, mdPFC-Pu, mdTH-pIC, and mdTH-OFC. Additionally, a few pair-wise FCs became even negative after stimulation: pCC-OFC, dpCC-pIC, AM-pIC, and AM-SAC. The results indicate that NAc-DBS, in general, have an inhibitory effect on major inter-ROI networks after acute stimulation; however, the modulation effect of NAc-DBS could also vary depending on the network being considered.

3.6 | The relationship between poststimulation FC change and strength of resting-state FC

While it is not surprising that stimulation could alter the functional connectivity between ROIs, further results showed that the extent of FC change was correlated with the rsFC and the strength of co-activation (Figure 9). A positively linear relationship was found between the change in FC in poststimulation and rsFC ($r = 0.82$, $p < .05$, $s = 0.54$), and stimulation-state FC ("co-activation") in ROIs ($r = 0.56$, $p < .05$, $s = 0.3$), indicating that the effectiveness of stimulation-induced modulation may vary depending on the rsFC.

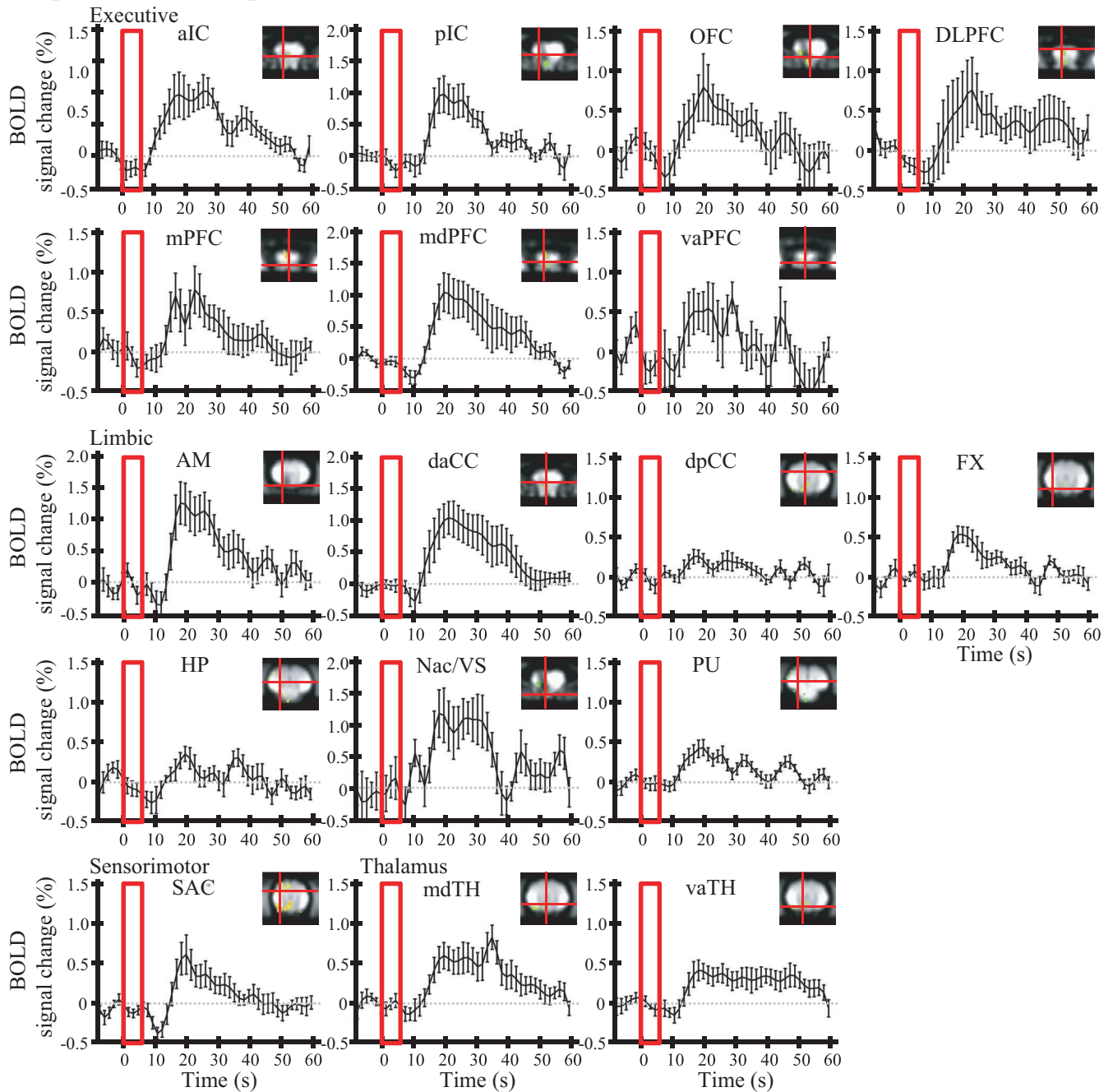
3.7 | Assessment of image artifacts induced by electric current

While it is known that the metal components of the DBS electrode can cause magnetic susceptibility artifacts as demonstrated by marked signal reductions in MR images near the implantation site (Settell et al., 2017), it is also possible that the electrical current of DBS could induce an additional image artifact, that is, increasing the size of the signal dropout area. The variation in image signal intensity was assessed near the signal dropout region during stimulation on and off periods; however, no statistically significant difference in signal intensity was found between stimulation on and off blocks (Figure 10). It therefore appears that the impact of electric current on the images is negligible.

4 | DISCUSSION

NAc-DBS-induced BOLD activation occurs not only near the stimulation locus (NAc), but also in the distal regions across multiple functional networks that include ipsilateral prefrontal, limbic, thalamic, and sensorimotor areas. While the patterns and extent of BOLD activation were consistent with previous results in pig models and in human studies (Gibson et al., 2016; Knight et al., 2013; Rauch et al., 1994), previous studies have not addressed the mechanism involved in the propagating effect NAc-DBS in the global brain. In our study, several ROIs lacking direct anatomical connections to the NAc showed temporally synchronized BOLD activity during stimulation ("co-activation"), indicating

(a) Ipsilateral hemisphere

 Stim.


(b) Contralateral hemisphere

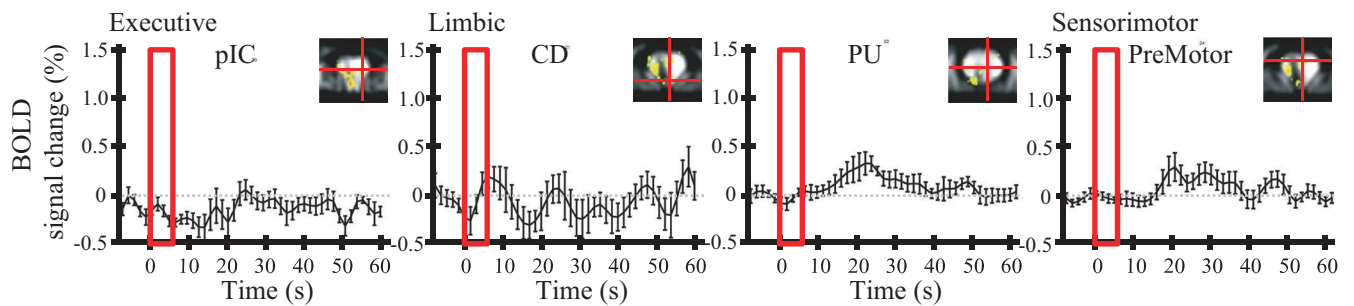
 Stim.


FIGURE 4 Time courses for the NAc-DBS-induced BOLD response in the ROIs (all subject averaged, $n = 8$) in (a) ipsilateral and (b) contralateral hemisphere. Six-second stimulation period is denoted by red bars. The error bars indicate the ± 1 standard error of the mean (SEM) of the BOLD signal. The location of each ROI is depicted in the upper right corner of individual figures. For the coordinates, see Table 1. NAc-DBS evoked robust BOLD responses, characterized by an initial negative component followed by a peak (5 ± 3 s and 25 ± 5 s after stimulation onset, respectively). For abbreviations, see Appendix A

that an anatomical connection alone cannot explain the diffuse pattern induced in a global brain. We therefore suggest that functional connectivity between stimulation locus and individual ROI and between ROIs likely play a crucial role in facilitating and propagating the DBS effect in distal brain regions.

4.1 | Anatomy and functional connectivity of nucleus accumbens (NAc)

Our resting-state analysis showed that NAc has significant resting-state functional connectivity (rsFC) with the medial portion of the prefrontal cortex (OFC and mdPFC), cingulate cortex, insular cortex, and limbic substructures. These results indicate the presence of significant functional coupling between NAc and an executive network, which is not irrelevant to its anatomical position that links the prefrontal cortex and basal ganglia complex (Brog, Salyapongse, Deutch, & Zahm, 1993; Haber, Kim, Maily, & Calzavara, 2006; Leh et al., 2007). NAc pathways play a key role in the development of reward-guided behavior by associating reward information with motivational and emotional features of sensory inputs (Groenewegen, Wright, Beijer, & Voorn, 1999; O'Doherty, 2004; Reiss et al., 2005), that is, perceptual learning between visual stimuli and esthetic music reward enhanced the strength of FC between NAc and visual cortex (Salimpoor et al., 2013).

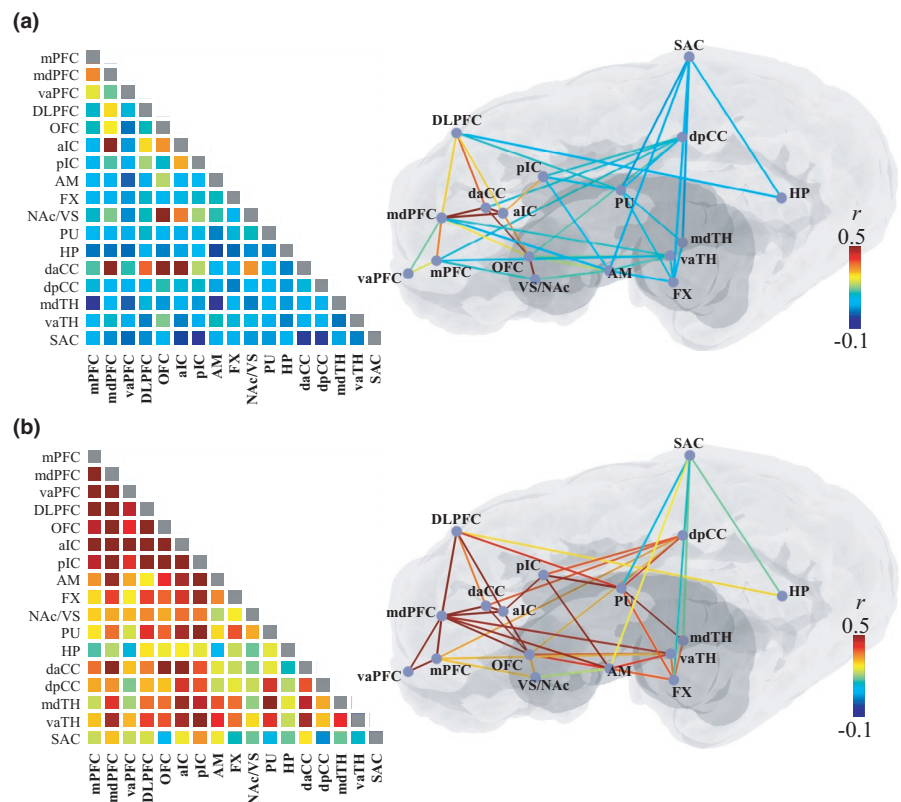
4.2 | Local neuromodulatory effects of NAc-DBS

Electrical stimulation directly modulates neuronal activity near the area of electrode implantation. Stimulation altered the spike rate of neurons and their firing pattern near stimulation locus (Anderson & Mullins, 2003; Dostrovsky & Lozano, 2002; Hashimoto, Elder, Okun, Patrick, & Vitek, 2003; McConnell, So, Hilliard, Lopomo, & Grill, 2012). Computation modeling simulated the extent of local effect (i.e., volume of tissue activated) (Butson & McIntyre, 2008; McIntyre & Grill, 1999). Our results also show that NAc-DBS evoked the diffuse activation of BOLD at the outside of the implantation locus (Figure 3). Thus, the findings suggest that the electric field likely extends from the implantation locus to adjacent subcortical tissues of the NAc, presumably through the local neuronal network, although the extent may depend on the stimulation parameters being applied (e.g., voltage and frequency) (Paek et al., 2015; Settell et al., 2017).

4.3 | Global neuromodulatory effects of NAc-DBS

The modulation of electrical stimulation could be limited to a subset of afferent neurons (Canteras, Shammah-Lagnado, Silva, & Ricardo, 1990); therefore, propagation of the effect to distal areas would be probabilistic and sparse in time (Chomiak & Hu, 2007;

FIGURE 5 Pair-wise functional connectivity (FC) is shown in the color encoded matrix (left) and illustrated with lines on a schematic brain diagram (right): (a) resting-state functional connectivity (rsFC) and (b) stimulation-state FC ("co-activation"). Colors indicate the group-averaged Pearson's correlation coefficient (r), ranging between -0.1 and 0.5 . Significant resting or stimulation-state functional connectivity ($p < .05$) is presented as colored lines on the brain illustration. Significant resting-state correlations were found between NAc and multiple cortical and subcortical ROIs. During a stimulation period, multiple ROIs evoked highly significantly correlated BOLD signal activity at $p < .05$ ("co-activation"). See for the abbreviations in Appendix A



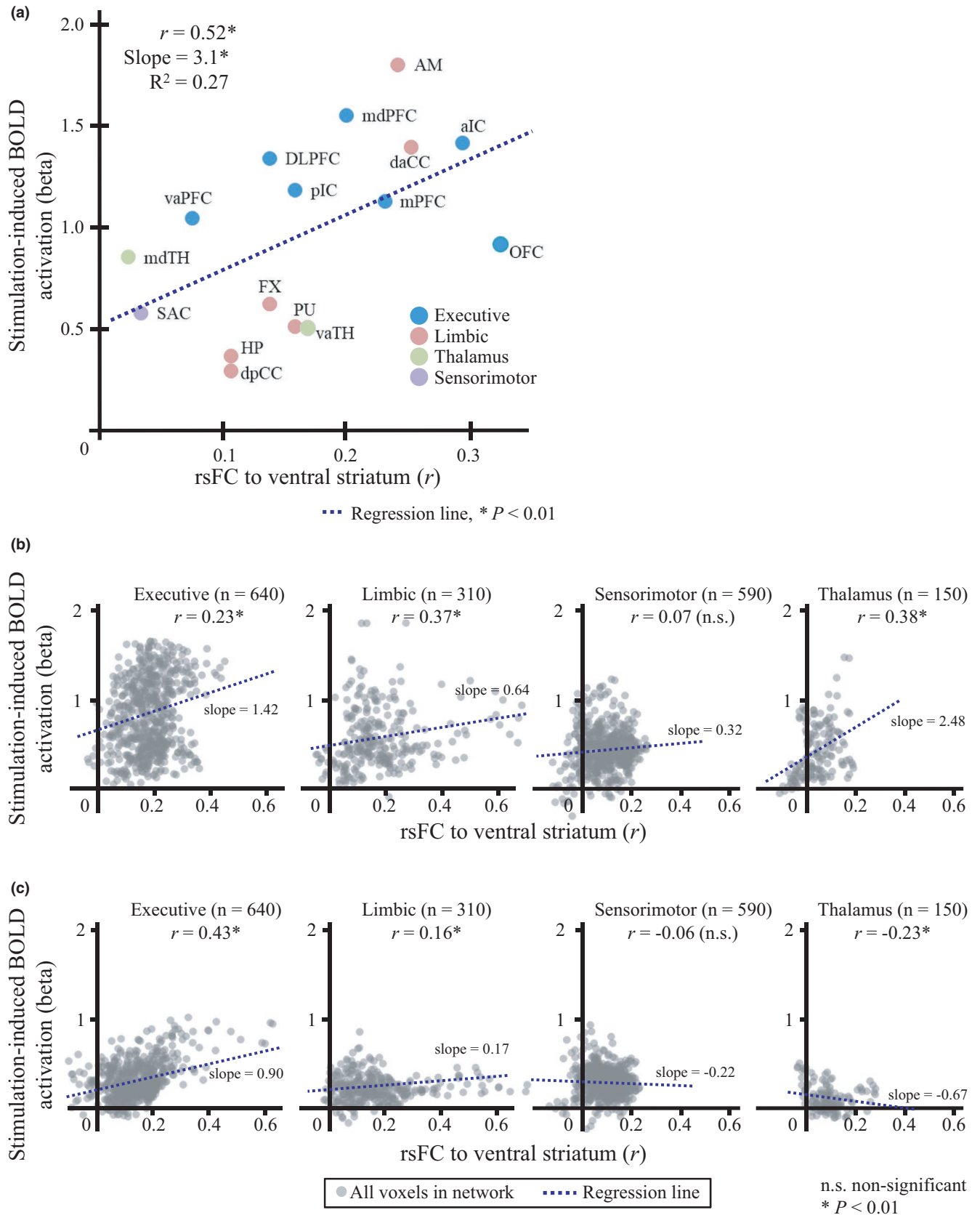


FIGURE 6 The relationship between resting-state functional connectivity (rsFC) to the location of the stimulation (rsFC-to-NAc) and BOLD activation in (a) the ROIs, and all other voxels in (b) ipsilateral (c) and contralateral functional networks. The horizontal and vertical axes denote the rsFC (group-averaged Pearson's correlation coefficient) of each ROI or voxel to NAc and the amplitude of BOLD activation (beta coefficient). The slope (s) of the linear regression is shown as a blue dotted line. Asterisks indicate a significant correlation between rsFC-to-NAc and BOLD activation in a given ROI or voxel of network. A significant linear relationship was found in the ROIs and voxels in ipsilateral functional networks. For the abbreviations, see Appendix A

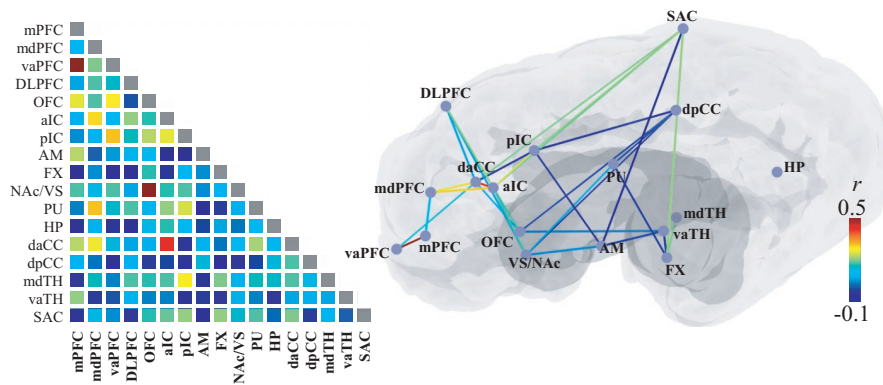


FIGURE 7 Pair-wise functional connectivity (FC) during the poststimulation period presented in the color encoded matrix (left) and illustrated with lines on a schematic brain diagram (right). Colors indicate the group-averaged Pearson's correlation coefficient (r), ranging between -0.1 and 0.5 . A significant change in FC was found in subcortical ROI pairs ($p < .05$), shown as with colored lines on the brain illustration. NAc-DBS suppresses functional connectivity between the ROIs and even alter the direction of connectivity from the positive to the negative in some ROI pairs. See for the abbreviations in Appendix A

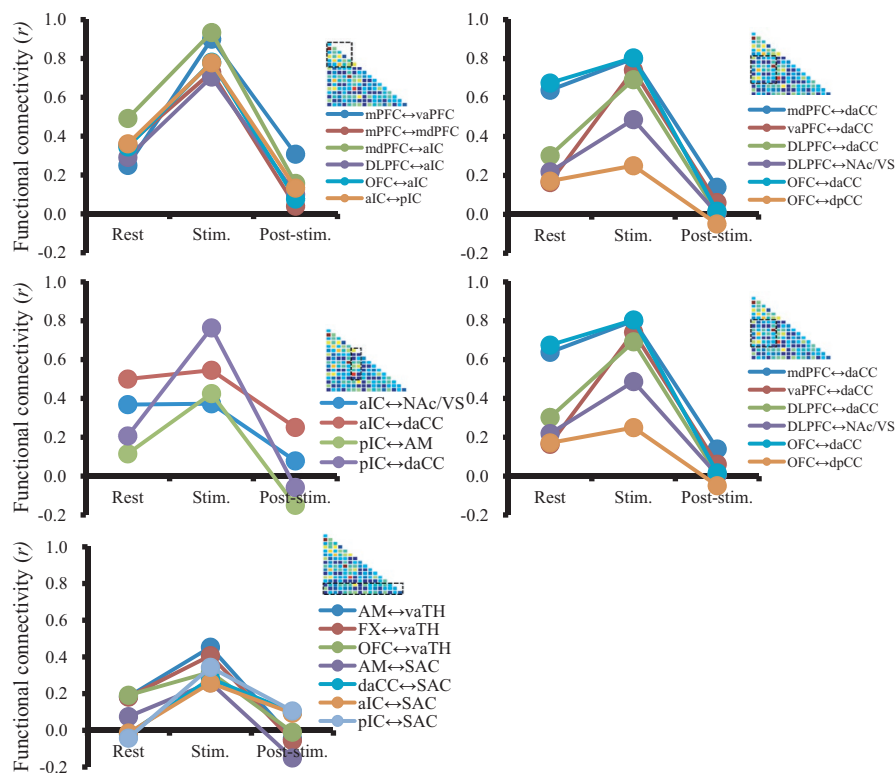


FIGURE 8 Significant changes in pair-wise functional connectivity across resting, stimulation, and poststimulation states. The ROI pairs were grouped according to internetwork combinations for visualization (executive-executive, executive-limbic, insular-limbic, limbic-limbic, and limbic-others). The horizontal axis indicates three states, and the vertical axis indicates the functional connectivity (r). The poststimulation correlation coefficient matrix is shown on the upper right corner for reference. Pair-wise FC is increased during the stimulation period ("co-activation") and decreased in poststimulation state ("inhibition"). See for the abbreviations in Appendix A

Hammond, Ammari, Bioulac, & Garcia, 2008). Such a limited local effect appears to somehow be in conflict with previous and present functional imaging results, wherein the DBS effect indeed extends to many distal regions. DBS-fMRI studies have shown that DBS evokes changes in the cerebral metabolic rate and BOLD signal in broad cortical and subcortical areas (Asanuma et al., 2006; Fukuda et al., 2004; Haslinger et al., 2003; Jech et al., 2001; Le Jeune et al., 2010; Min et al., 2012; Rezai et al., 1999). Thus, these results

suggest that a certain neurobiological mechanism is operative that allows the local modulatory effect to propagate to the global brain.

4.4 | The role of functional connectivity in the propagation of NAc-DBS effect

Some activated areas, on the one hand, appear to be anatomically linked to the NAc. For example, an anatomical connection has

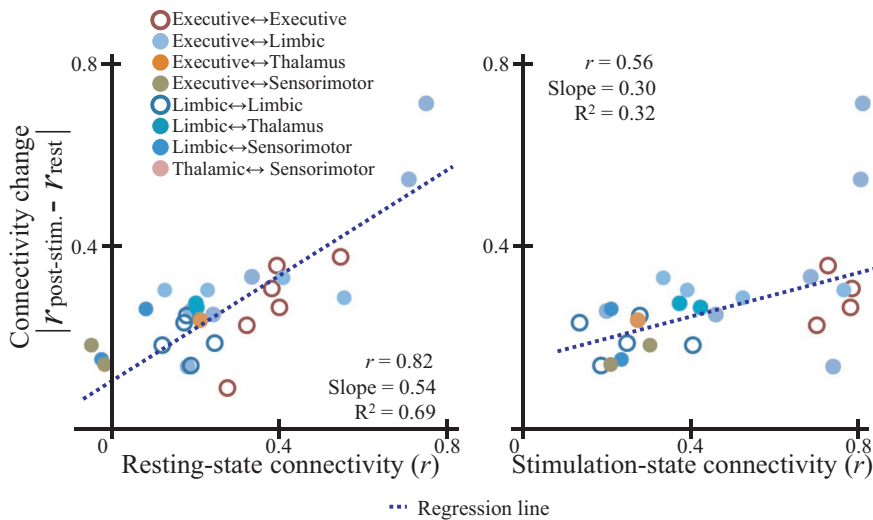
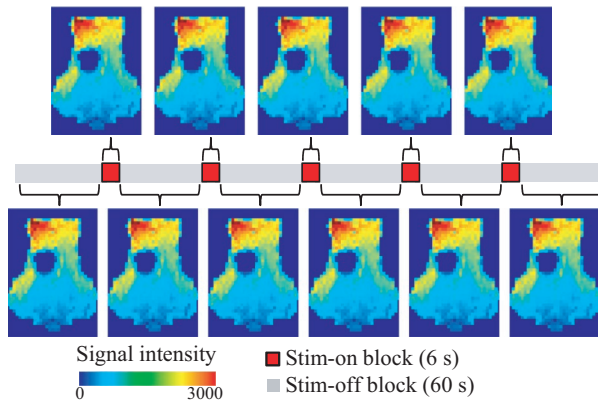


FIGURE 9 Relationship between inter-ROI resting-state functional connectivity and change in functional connectivity in the poststimulation state. Each circle represented an individual ROI pair, in which filled and unfilled circles differentiate the pairs between inter- and intranetwork. A significant, positive relationship was found between pair-wise FC change and resting-state FC ($r = 0.82$, slope = 0.54, $p < .001$) and stimulation-state FC ($r = 0.56$, slope = 0.25, $p < .01$), respectively, demonstrating that resting and stimulation-state connectivity could predict FC change in a given ROI pair

(a) Block-average slice images



(b) Cross-section signal intensity

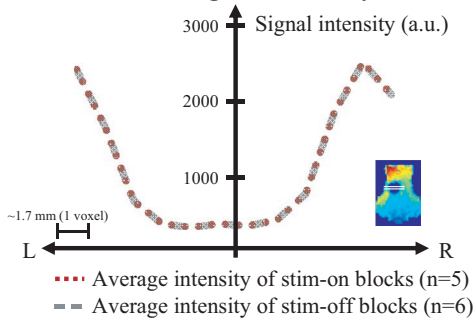


FIGURE 10 Assessment of an electric current-induced EPI image artifact (a single subject). The intensity of the image signals was compared between electrical stimulation ON and OFF periods (a) block averaged axial image slices in stimulation ON and OFF block and (b) one dimensional plot of signal intensity across the “signal dropout region” for each condition. The horizontal axis denotes the distance from the center of signal dropout region, and the vertical axis denotes the voxel signal intensity. No significant difference in EPI images was found between stimulation ON and OFF periods, indicating that the influence of the electric current might be negligible

been identified between the NAc and prefrontal regions, as shown by DTI investigations (Britt et al., 2012; Brunenberg et al., 2012; Leh et al., 2007; Lehericy et al., 2004). Some networks have been identified as involving the basal ganglia complex, that is, an “indirect” (Damoiseaux & Greicius, 2009; Montaron, Deniau, Menetrey, Glowinski, & Thierry, 1996), “hyper-direct” pathway (Brunenberg et al., 2012; Nambu, Tokuno, & Takada, 2002), or the recurrent loops (Leblois, Boraud, Meissner, Bergman, & Hansel, 2006). On the other hand, however, the anatomical connection cannot fully explain the highly spread pattern of activation across large-scale brain networks. Here, our results showed that the stronger the rsFC of a given region to the NAc was, the larger was the induced BOLD response (Figure 6). Thus, a functional connection that originated from the stimulation locus is highly likely to be the source of the BOLD activation pattern observed in the global brain. Furthermore, a greater FC change was observed in the poststimulation period when the rsFC in the two regions was stronger, supporting the idea that the rsFC may propagate the modulation effect in distal regions from the stimulation locus.

4.5 | Functional connectivity change after NAc-DBS

Many inter-regional functional connectivity (FC) changes decrease after stimulation (Figure 7), indicating that the NAc-DBS tends to have an inhibitory effect on functional connections. However, the magnitudes of reduction were not equal in the ROIs, and in some cases, the direction of functional coupling became reversed (i.e., negative correlation) or increased compared with the baseline condition (Figure 8). These results suggest that the DBS effect varies depending on the network being considered (Albaugh et al., 2016). It is generally thought that the DBS exerts its therapeutic effect by regularizing or normalizing a pathological oscillation in large-scale networks (Chicken & Nambu, 2014; McIntyre & Hahn, 2010; Rosenbaum et al., 2014; Vitek, 2002). In line with the “network effect” perspective, we suggest that a variety of effects (inhibition or facilitation of functional connectivity) of DBS

may reflect its regularizing efficacy for inter-regional neuronal transmission, rather than simply inhibiting network activity.

The current steering technique with a novel lead design (Lehto et al., 2017; Martens et al., 2011) enables the shape of the electric field to be adjusted by the injection of an asymmetric current, thus providing better control of the DBS-induced electric field (Butson & McIntyre, 2008). Functional imaging would then be better incorporated in terms of elucidating local and global modulation effects by adopting such selective stimulation to localize effects on the surrounding tissue of the NAc.

Note that we measured FC changes after a short period of stimulation (6 s) for a relatively short period of time (30 s) compared with the chronic DBS condition. Thus, the FC changes in the present study might reflect the acute effect of the NAc-DBS. Further studies with a longer duration of stimulation would provide a more complete understanding of the effect of chronic DBS.

4.6 | The influence of anesthesia on stimulation-associated BOLD activity

The level of sedation (Liu, Zhu, Zhang, & Chen, 2013) and type of anesthetic agent (Angenstein, Kammerer, & Scheich, 2009; Angenstein, Krautwald, & Scheich, 2010) can have an influence on the BOLD hemodynamic response. Higher isoflurane concentrations (the dose over 1.8%) tend to suppress BOLD activity and results in a decrease in spatial specificity with different functional networks being dissolved during resting states (Liu et al., 2013). A burst suppression of the neuronal population was found in cases where high doses of isoflurane were used (Liu, Zhu, Zhang, & Chen, 2010; Vincent et al., 2007), suggesting that isoflurane as an anesthetic agent may have an impact on both hemodynamic and neuronal activity. In contrast to the high concentration, BOLD activation was preserved when a relatively lower dose (<1.3%) was used (Knight et al., 2013; Min et al., 2012; Paek et al., 2015), suggesting that the impact of isoflurane anesthesia would be less influential or negligible when a lower dose is used. It should be noted here that we cannot completely rule out the possibility that BOLD activation and the rsFC measurements were underestimated due to anesthesia. Nevertheless, we observed a robust amplitude (0.3%–1.3% signal change from the baseline) and temporal pattern of BOLD activation that are consistent with previous fMRI results (Knight et al., 2013; Min et al., 2012; Paek et al., 2015; Settell et al., 2017).

4.7 | Clinical implications for human NAc-DBS and Applications for DBS-fMRI

Dysfunctional functional connectivity between the NAc and various brain regions has been implicated in a number of neuropsychiatric disorders (Da Cunha et al., 2015). Combining NAc-DBS with functional imaging allows causal relationships between the stimulation and modulation of functional networks to be identified, thus providing insights into the underlying mechanisms responsible for

the therapeutic and adverse effects of NAc-DBS, particularly for neuropsychiatric disorders, for example, OCD and mood disorders (Bewernick et al., 2010; Bewernick, Kayser, Sturm, & Schlaepfer, 2012). Although our subjects were healthy animals, a large animal model can be implicated as a model for the human brain (Van Gompel et al., 2011), providing insights into how the modulation of these networks might underlie the potential therapeutic efficacy of human NAc-DBS.

ACKNOWLEDGMENTS

This work was supported by the National Institutes of Health (NIH CO6 RR018898 and NIH R01 NS70872), Hanyang University (HY-2019), and the Grainger Foundation.

CONFLICT OF INTEREST

The author(s) declare that there were no conflicts of interest with respect to the authorship or the publication of this article.

AUTHOR CONTRIBUTIONS

All of the authors contributed to the study design. Data collection and analyses were performed by S. Cho, M. In, H. Min, and H. J. Jo. The manuscript was written by S. Cho, J. T. Hachmann, I. Balzekas, L. G. Andres-Beck, and H. J. Jo in consultation with other authors. All the authors approved the final version of the manuscript for submission.

DATA AVAILABILITY STATEMENT

The data that support the findings of this study are openly available in Data for: Resting-state functional connectivity modulates the BOLD activation induced by nucleus accumbens stimulation in the swine brain at <http://dx.doi.org/10.17632/r6f82ypfv.3> (Cho, 2019).

ORCID

Shinho Cho  <https://orcid.org/0000-0002-3886-3106>

Hang Joon Jo  <https://orcid.org/0000-0002-9180-3831>

REFERENCES

- Albaugh, D. L., Salzwedel, A., Van Den Berge, N., Gao, W., Stuber, G. D., & Shih, Y.-Y.-I. (2016). Functional magnetic resonance imaging of electrical and optogenetic deep brain stimulation at the rat nucleus accumbens. *Scientific Reports*, *6*, 31613. <https://doi.org/10.1038/srep31613>
- Anderson, K. E., & Mullins, J. (2003). Behavioral changes associated with deep brain stimulation surgery for Parkinson's disease. *Current Neurology and Neuroscience Reports*, *3*(4), 306–313. <https://doi.org/10.1007/s11910-003-0007-z>
- Angenstein, F., Kammerer, E., & Scheich, H. (2009). The BOLD response in the rat hippocampus depends rather on local processing of signals

- than on the input or output activity. A combined functional MRI and electrophysiological study. *Journal of Neuroscience*, 29(8), 2428–2439.
- Angenstein, F., Krautwald, K., & Scheich, H. (2010). The current functional state of local neuronal circuits controls the magnitude of a BOLD response to incoming stimuli. *NeuroImage*, 50(4), 1364–1375. <https://doi.org/10.1016/j.neuroimage.2010.01.070>
- Asanuma, K., Tang, C., Ma, Y., Dhawan, V., Mattis, P., Edwards, C., ... Eidelberg, D. (2006). Network modulation in the treatment of Parkinson's disease. *Brain*, 129(10), 2667–2678. <https://doi.org/10.1093/brain/awl162>
- Baxter, L. R., Schwartz, J. M., Bergman, K. S., Szuba, M. P., Guze, B. H., Mazziotta, J. C., ... Munford, P. (1992). Caudate glucose metabolic rate changes with both drug and behavior therapy for obsessive-compulsive disorder. *Archives of General Psychiatry*, 49(9), 681–689. <https://doi.org/10.1001/archpsyc.1992.01820090009002>
- Benabid, A. L. (2003). Deep brain stimulation for Parkinson's disease. *Current Opinion in Neurobiology*, 13(6), 696–706. <https://doi.org/10.1016/j.conb.2003.11.001>
- Benabid, A. L., Pollak, P., Hoffmann, D., Gervason, C., Hommel, M., Perret, J., ... Gao, D. (1991). Long-term suppression of tremor by chronic stimulation of the ventral intermediate thalamic nucleus. *The Lancet*, 337(8738), 403–406.
- Bewernick, B. H., Hurlmann, R., Matusch, A., Kayser, S., Grubert, C., Hadryiewicz, B., ... Schlaepfer, T. E. (2010). Nucleus accumbens deep brain stimulation decreases ratings of depression and anxiety in treatment-resistant depression. *Biological Psychiatry*, 67(2), 110–116. <https://doi.org/10.1016/j.biopsych.2009.09.013>
- Bewernick, B. H., Kayser, S., Sturm, V., & Schlaepfer, T. E. (2012). Long-term effects of nucleus accumbens deep brain stimulation in treatment-resistant depression: Evidence for sustained efficacy. *Neuropsychopharmacology*, 37(9), 1975–1985. <https://doi.org/10.1038/npp.2012.44>
- Birn, R. M., Diamond, J. B., Smith, M. A., & Bandettini, P. A. (2006). Separating respiratory-variation-related fluctuations from neuronal-activity-related fluctuations in fMRI. *NeuroImage*, 31(4), 1536–1548. <https://doi.org/10.1016/j.neuroimage.2006.02.048>
- Biswal, B., Zerrin Yetkin, F., Haughton, V. M., & Hyde, J. S. (1995). Functional connectivity in the motor cortex of resting human brain using echo-planar MRI. *Magnetic Resonance in Medicine*, 34(4), 537–541. <https://doi.org/10.1002/mrm.1910340409>
- Britt, J. P., Benaliouf, F., McDevitt, R. A., Stuber, G. D., Wise, R. A., & Bonci, A. (2012). Synaptic and behavioral profile of multiple glutamatergic inputs to the nucleus accumbens. *Neuron*, 76(4), 790–803. <https://doi.org/10.1016/j.neuron.2012.09.040>
- Brog, J. S., Salyapongse, A., Deutch, A. Y., & Zahm, D. S. (1993). The patterns of afferent innervation of the core and shell in the “accumbens” part of the rat ventral striatum: Immunohistochemical detection of retrogradely transported fluoro-gold. *Journal of Comparative Neurology*, 338(2), 255–278. <https://doi.org/10.1002/cne.903380209>
- Brunenberg, E. J. L., Moeskops, P., Backes, W. H., Pollo, C., Cammoun, L., Vilanova, A., ... Platel, B. (2012). Structural and resting state functional connectivity of the subthalamic nucleus: Identification of motor STN parts and the hyperdirect pathway. *PLoS ONE*, 7(6), e39061. <https://doi.org/10.1371/journal.pone.0039061>
- Butson, C. R., & McIntyre, C. C. (2008). Current steering to control the volume of tissue activated during deep brain stimulation. *Brain Stimulation*, 1(1), 7–15. <https://doi.org/10.1016/j.brs.2007.08.004>
- Canteras, N. S., Shammah-Lagnado, S. J., Silva, B. A., & Ricardo, J. A. (1990). Afferent connections of the subthalamic nucleus: A combined retrograde and anterograde horseradish peroxidase study in the rat. *Brain Research*, 513(1), 43–59. [https://doi.org/10.1016/0006-8993\(90\)91087-W](https://doi.org/10.1016/0006-8993(90)91087-W)
- Cauda, F., Cavanna, A. E., D'Agata, F., Sacco, K., Duca, S., & Geminiani, G. C. (2011). Functional connectivity and coactivation of the nucleus accumbens: A combined functional connectivity and structure-based meta-analysis. *Journal of Cognitive Neuroscience*, 23(10), 2864–2877. <https://doi.org/10.1162/jocn.2011.21624>
- Chicken, S., & Nambu, A. (2014). Disrupting neuronal transmission: mechanism of DBS?. *Frontiers in Systems Neuroscience*, 8, 33.
- Cho, S. (2019). Data for: Resting-state functional connectivity modulates the BOLD activation induced by nucleus accumbens stimulation in the swine brain. Mendeley Data, V3, <https://doi.org/10.17632/r6f82ypfvf.3>
- Chomiak, T., & Hu, B. (2007). Axonal and somatic filtering of antidromically evoked cortical excitation by simulated deep brain stimulation in rat brain. *The Journal of Physiology*, 579(2), 403–412. <https://doi.org/10.1113/jphysiol.2006.124057>
- Coubes, P., Cif, L., El Fertit, H., Hemm, S., Vayssiere, N., Serrat, S., ... Frerebeau, P. (2004). Electrical stimulation of the globus pallidus internus in patients with primary generalized dystonia: Long-term results. *Journal of Neurosurgery*, 101(2), 189–194. <https://doi.org/10.3171/jns.2004.101.2.0189>
- Cox, R. W. (1996). AFNI: Software for analysis and visualization of functional magnetic resonance neuroimages. *Computers and Biomedical Research*, 29(3), 162–173. <https://doi.org/10.1006/cbmr.1996.0014>
- Da Cunha, C., Boschen, S. L., Gómez-A, A., Ross, E. K., Gibson, W. S. J., Min, H.-K., ... Blaha, C. D. (2015). Toward sophisticated basal ganglia neuromodulation: Review on basal ganglia deep brain stimulation. *Neuroscience & Biobehavioral Reviews*, 58, 186–210. <https://doi.org/10.1016/j.neubiorev.2015.02.003>
- Damoiseaux, J. S., & Greicius, M. D. (2009). Greater than the sum of its parts: A review of studies combining structural connectivity and resting-state functional connectivity. *Brain Structure and Function*, 213(6), 525–533. <https://doi.org/10.1007/s00429-009-0208-6>
- Davey, C. E., Grayden, D. B., Egan, G. F., & Johnston, L. A. (2013). Filtering induces correlation in fMRI resting state data. *NeuroImage*, 64, 728–740. <https://doi.org/10.1016/j.neuroimage.2012.08.022>
- Deep-Brain Stimulation for Parkinson's Disease Study Group (2001). Deep-brain stimulation of the subthalamic nucleus or the pars interna of the globus pallidus in Parkinson's disease. *New England Journal of Medicine*, 2001(345), 956–963.
- Denys, D., Mantione, M., Figee, M., van den Munckhof, P., Koerselman, F., Westenberg, H., ... Schuurman, R. (2010). Deep brain stimulation of the nucleus accumbens for treatment-refractory obsessive-compulsive disorder. *Archives of General Psychiatry*, 67(10), 1061–1068. <https://doi.org/10.1001/archgenpsychiatry.2010.122>
- Di Martino, A., Scheres, A., Margulies, D. S., Kelly, A. M. C., Uddin, L. Q., Shehzad, Z., ... Milham, M. P. (2008). Functional connectivity of human striatum: A resting state fMRI study. *Cerebral Cortex*, 18(12), 2735–2747. <https://doi.org/10.1093/cercor/bhn041>
- Dostrovsky, J. O., & Lozano, A. M. (2002). Mechanisms of deep brain stimulation. *Movement Disorders*, 17(S3), S63–S68. <https://doi.org/10.1002/mds.10143>
- Figee, M., Luigjes, J., Smolders, R., Valencia-Alfonso, C.-E., van Wingen, G., de Kwaasteniet, B., ... Denys, D. (2013). Deep brain stimulation restores frontostriatal network activity in obsessive-compulsive disorder. *Nature Neuroscience*, 16(4), 386–387. <https://doi.org/10.1038/nn.3344>
- Fox, M. D., Halko, M. A., Eldaief, M. C., & Pascual-Leone, A. (2012). Measuring and manipulating brain connectivity with resting state functional connectivity magnetic resonance imaging (fcMRI) and transcranial magnetic stimulation (TMS). *NeuroImage*, 62(4), 2232–2243. <https://doi.org/10.1016/j.neuroimage.2012.03.035>
- Fukuda, M., Barnes, A., Simon, E. S., Holmes, A., Dhawan, V., Giladi, N., ... Eidelberg, D. (2004). Thalamic stimulation for parkinsonian tremor: Correlation between regional cerebral blood flow and physiological tremor characteristics. *NeuroImage*, 21(2), 608–615. <https://doi.org/10.1016/j.neuroimage.2003.09.068>
- Gibson, W. S., Cho, S., Abulseoud, O. A., Gorny, K. R., Felmler, J. P., Welker, K. M., ... Lee, K. H. (2016). The impact of mirth-inducing ventral

- striatal deep brain stimulation on functional and effective connectivity. *Cerebral Cortex*, 27, 2183–2194. <https://doi.org/10.1093/cercor/bhw074>
- Greenberg, B. D., Gabriels, L. A., Malone, D. A., Rezaei, A. R., Friehs, G. M., Okun, M. S., ... Nuttin, B. J. (2010). Deep brain stimulation of the ventral internal capsule/ventral striatum for obsessive-compulsive disorder: Worldwide experience. *Molecular Psychiatry*, 15(1), 64–79. <https://doi.org/10.1038/mp.2008.55>
- Greenberg, B. D., Malone, D. A., Friehs, G. M., Rezaei, A. R., Kubu, C. S., Malloy, P. F., ... Rasmussen, S. A. (2006). Three-year outcomes in deep brain stimulation for highly resistant obsessive-compulsive disorder. *Neuropsychopharmacology*, 31(11), 2384–2393. <https://doi.org/10.1038/sj.npp.1301165>
- Greicius, M. D., Krasnow, B., Reiss, A. L., & Menon, V. (2003). Functional connectivity in the resting brain: A network analysis of the default mode hypothesis. *Proceedings of the National Academy of Sciences of the USA*, 100(1), 253–258. <https://doi.org/10.1073/pnas.0135058100>
- Groenewegen, H. J., Wright, C. I., Beijer, A. V., & Voorn, P. (1999). Convergence and segregation of ventral striatal inputs and outputs. *Annals of the New York Academy of Sciences*, 877(1), 49–63. <https://doi.org/10.1111/j.1749-6632.1999.tb09260.x>
- Haber, S. N., Kim, K.-S., Maily, P., & Calzavara, R. (2006). Reward-related cortical inputs define a large striatal region in primates that interface with associative cortical connections, providing a substrate for incentive-based learning. *Journal of Neuroscience*, 26(32), 8368–8376. <https://doi.org/10.1523/JNEUROSCI.0271-06.2006>
- Hamani, C., Pilitsis, J., Rughani, A. I., Rosenow, J. M., Patil, P. G., Slavin, K. S., ... Kalkanis, S. (2014). Deep brain stimulation for obsessive-compulsive disorder: Systematic review and evidence-based guideline sponsored by the American Society for Stereotactic and Functional Neurosurgery and the Congress of Neurological Surgeons (CNS) and endorsed by the CNS and American Association of Neurological Surgeons. *Neurosurgery*, 75(4), 327–333. <https://doi.org/10.1227/NEU.0000000000000499>
- Hammond, C., Ammari, R., Bioulac, B., & Garcia, L. (2008). Latest view on the mechanism of action of deep brain stimulation. *Movement Disorders*, 23(15), 2111–2121. <https://doi.org/10.1002/mds.22120>
- Hashimoto, T., Elder, C. M., Okun, M. S., Patrick, S. K., & Vitek, J. L. (2003). Stimulation of the subthalamic nucleus changes the firing pattern of pallidal neurons. *The Journal of Neuroscience*, 23(5), 1916–1923. <https://doi.org/10.1523/JNEUROSCI.23-05-01916.2003>
- Haslinger, B., Boecker, H., Büchel, C., Vesper, J., Tronnier, V. M., Pfister, R., ... Ceballos-Baumann, A. O. (2003). Differential modulation of subcortical target and cortex during deep brain stimulation. *NeuroImage*, 18(2), 517–524. [https://doi.org/10.1016/S1053-8119\(02\)00043-5](https://doi.org/10.1016/S1053-8119(02)00043-5)
- Horn, A., & Kühn, A. A. (2015). Lead-DBS: A toolbox for deep brain stimulation electrode localizations and visualizations. *NeuroImage*, 107, 127–135. <https://doi.org/10.1016/j.neuroimage.2014.12.002>
- Houeto, J.-L., Karachi, C., Mallet, L., Pillon, B., Yelnik, J., Mesnage, V., ... Damier, P. (2005). Tourette's syndrome and deep brain stimulation. *Journal of Neurology, Neurosurgery & Psychiatry*, 76(7), 992–995. <https://doi.org/10.1136/jnnp.2004.043273>
- Jech, R., Urgošik, D., Tintěra, J., Nebuželský, A., Krásenský, J., Liščák, R., ... Růžička, E. (2001). Functional magnetic resonance imaging during deep brain stimulation: A pilot study in four patients with Parkinson's disease. *Movement Disorders*, 16(6), 1126–1132. <https://doi.org/10.1002/mds.1217>
- Knight, E. J., Min, H.-K., Hwang, S.-C., Marsh, M. P., Paek, S., Kim, I., ... Lee, K. H. (2013). Nucleus accumbens deep brain stimulation results in insula and prefrontal activation: A large animal fMRI study. *PLoS ONE*, 8(2), e56640. <https://doi.org/10.1371/journal.pone.0056640>
- Knutson, B., Adams, C. M., Fong, G. W., & Hommer, D. (2001). Anticipation of increasing monetary reward selectively recruits nucleus accumbens. *Journal of Neuroscience*, 21(16), RC159. <https://doi.org/10.1523/JNEUROSCI.21-16-j0002.2001>
- Krack, P., Hariz, M. I., Baunez, C., Guridi, J., & Obeso, J. A. (2010). Deep brain stimulation: From neurology to psychiatry? *Trends in Neurosciences*, 33(10), 474–484. <https://doi.org/10.1016/j.tins.2010.07.002>
- Kuhn, J., Bauer, R., Pohl, S., Lenartz, D., Huff, W., Kim, E. H., ... Sturm, V. (2009). Observations on unaided smoking cessation after deep brain stimulation of the nucleus accumbens. *European Addiction Research*, 15(4), 196–201. <https://doi.org/10.1159/000228930>
- Kuhn, J., Lenartz, D., Huff, W., Lee, S., Koulousakis, A., Klosterkoetter, J., & Sturm, V. (2007). Remission of alcohol dependency following deep brain stimulation of the nucleus accumbens: Valuable therapeutic implications? *Journal of Neurology, Neurosurgery & Psychiatry*, 78(10), 1152–1153. <https://doi.org/10.1136/jnnp.2006.113092>
- Le Jeune, F., Vérin, M., N'Diaye, K., Drapier, D., Leray, E., Du Montcel, S. T., ... Millet, B. (2010). Decrease of prefrontal metabolism after subthalamic stimulation in obsessive-compulsive disorder: A positron emission tomography study. *Biological Psychiatry*, 68(11), 1016–1022. <https://doi.org/10.1016/j.biopsych.2010.06.033>
- Leblois, A., Boraud, T., Meissner, W., Bergman, H., & Hansel, D. (2006). Competition between feedback loops underlies normal and pathological dynamics in the basal ganglia. *Journal of Neuroscience*, 26(13), 3567–3583. <https://doi.org/10.1523/JNEUROSCI.5050-05.2006>
- Leh, S. E., Ptito, A., Chakravarty, M. M., & Strafella, A. P. (2007). Frontostriatal connections in the human brain: A probabilistic diffusion tractography study. *Neuroscience Letters*, 419(2), 113–118. <https://doi.org/10.1016/j.neulet.2007.04.049>
- Lehéricy, S., Ducros, M., Van De Moortele, P.-F., Francois, C., Thivard, L., Poupon, C., ... Kim, D.-S. (2004). Diffusion tensor fiber tracking shows distinct corticostriatal circuits in humans. *Annals of Neurology*, 55(4), 522–529. <https://doi.org/10.1002/ana.20030>
- Lehto, L. J., Slopsema, J. P., Johnson, M. D., Shatillo, A., Teplitzky, B. A., Utecht, L., ... Gröhn, O. (2017). Orientation selective deep brain stimulation. *Journal of Neural Engineering*, 14(1), 016016.
- Liu, X., Zhu, X.-H., Zhang, Y., & Chen, W. (2010). Neural origin of spontaneous hemodynamic fluctuations in rats under burst – Suppression anesthesia condition. *Cerebral Cortex*, 21(2), 374–384. <https://doi.org/10.1093/cercor/bhq105>
- Liu, X., Zhu, X.-H., Zhang, Y., & Chen, W. (2013). The change of functional connectivity specificity in rats under various anesthesia levels and its neural origin. *Brain Topography*, 26(3), 363–377. <https://doi.org/10.1007/s10548-012-0267-5>
- Mallet, L., Polosan, M., Jaafari, N., Baup, N., Welter, M.-L., Fontaine, D., ... Pelissolo, A. (2008). Subthalamic nucleus stimulation in severe obsessive-compulsive disorder. *New England Journal of Medicine*, 359(20), 2121–2134. <https://doi.org/10.1056/NEJMoa0708514>
- Martens, H. C. F., Toader, E., Decré, M. M. J., Anderson, D. J., Vetter, R., Kipke, D. R., ... Vitek, J. L. (2011). Spatial steering of deep brain stimulation volumes using a novel lead design. *Clinical Neurophysiology*, 122(3), 558–566.
- Mayberg, H. S., Lozano, A. M., Voon, V., McNeely, H. E., Seminowicz, D., Hamani, C., ... Kennedy, S. H. (2005). Deep brain stimulation for treatment-resistant depression. *Neuron*, 45(5), 651–660. <https://doi.org/10.1016/j.neuron.2005.02.014>
- McConnell, G. C., So, R. Q., Hilliard, J. D., Lopomo, P., & Grill, W. M. (2012). Effective deep brain stimulation suppresses low-frequency network oscillations in the basal ganglia by regularizing neural firing patterns. *Journal of Neuroscience*, 32(45), 15657–15668. <https://doi.org/10.1523/JNEUROSCI.2824-12.2012>
- McCracken, C. B., & Grace, A. A. (2007). High-frequency deep brain stimulation of the nucleus accumbens region suppresses neuronal activity and selectively modulates afferent drive in rat orbitofrontal cortex in vivo. *Journal of Neuroscience*, 27(46), 12601–12610. <https://doi.org/10.1523/JNEUROSCI.3750-07.2007>

- McIntyre, C. C., & Grill, W. M. (1999). Excitation of central nervous system neurons by nonuniform electric fields. *Biophysical Journal*, 76(2), 878–888. [https://doi.org/10.1016/S0006-3495\(99\)77251-6](https://doi.org/10.1016/S0006-3495(99)77251-6)
- McIntyre, C. C., & Hahn, P. J. (2010). Network perspectives on the mechanisms of deep brain stimulation. *Neurobiology of Disease*, 38(3), 329–337. <https://doi.org/10.1016/j.nbd.2009.09.022>
- McIntyre, C. C., Mori, S., Sherman, D. L., Thakor, N. V., & Vitek, J. L. (2004). Electric field and stimulating influence generated by deep brain stimulation of the subthalamic nucleus. *Clinical Neurophysiology*, 115(3), 589–595. <https://doi.org/10.1016/j.clinph.2003.10.033>
- Min, H.-K., Hwang, S.-C., Marsh, M. P., Kim, I., Knight, E., Striemer, B., ... Lee, K. H. (2012). Deep brain stimulation induces BOLD activation in motor and non-motor networks: An fMRI comparison study of STN and EN/GPi DBS in large animals. *NeuroImage*, 63(3), 1408–1420. <https://doi.org/10.1016/j.neuroimage.2012.08.006>
- Min, H.-K., Ross, E. K., Lee, K. H., Dennis, K., Han, S. R., Jeong, J. H., ... Bennet, K. E. (2014). Subthalamic nucleus deep brain stimulation induces motor network BOLD activation: Use of a high precision MRI guided stereotactic system for nonhuman primates. *Brain Stimulation*, 7(4), 603–607. <https://doi.org/10.1016/j.brs.2014.04.007>
- Montaron, M., Deniau, J., Menetrey, A., Glowinski, J., & Thierry, A. (1996). Prefrontal cortex inputs of the nucleus accumbens-nigro-thalamic circuit. *Neuroscience*, 71(2), 371–382. [https://doi.org/10.1016/0306-4522\(95\)00455-6](https://doi.org/10.1016/0306-4522(95)00455-6)
- Morgane, P. J., Galler, J. R., & Mokler, D. J. (2005). A review of systems and networks of the limbic forebrain/limbic midbrain. *Progress in Neurobiology*, 75(2), 143–160.
- Nambu, A., Tokuno, H., & Takada, M. (2002). Functional significance of the cortico-subthalamo-pallidal ‘hyperdirect’ pathway. *Neuroscience Research*, 43(2), 111–117. [https://doi.org/10.1016/S0168-0102\(02\)00027-5](https://doi.org/10.1016/S0168-0102(02)00027-5)
- Nuttin, B., Cosyns, P., Demeulemeester, H., Gybels, J., & Meyerson, B. (1999). Electrical stimulation in anterior limbs of internal capsules in patients with obsessive-compulsive disorder. *The Lancet*, 354(9189), 1526. [https://doi.org/10.1016/S0140-6736\(99\)02376-4](https://doi.org/10.1016/S0140-6736(99)02376-4)
- O’Doherty, J., Dayan, P., Schultz, J., Deichmann, R., Friston, K., & Dolan, R. J. (2004). Dissociable roles of ventral and dorsal striatum in instrumental conditioning. *Science*, 304(5669), 452–454.
- Ogawa, S., Menon, R., Tank, D. W., Kim, S., Merkle, H., Ellermann, J., & Ugurbil, K. (1993). Functional brain mapping by blood oxygenation level-dependent contrast magnetic resonance imaging. A comparison of signal characteristics with a biophysical model. *Biophysical Journal*, 64(3), 803–812.
- Ogawa, S., Tank, D. W., Menon, R., Ellermann, J. M., Kim, S. G., Merkle, H., & Ugurbil, K. (1992). Intrinsic signal changes accompanying sensory stimulation: Functional brain mapping with magnetic resonance imaging. *Proceedings of the National Academy of Sciences of the USA*, 89(13), 5951–5955. <https://doi.org/10.1073/pnas.89.13.5951>
- Paek, S. B., Min, H.-K., Kim, I., Knight, E. J., Baek, J. J., Bieber, A. J., ... Chang, S.-Y. (2015). Frequency-dependent functional neuromodulatory effects on the motor network by ventral lateral thalamic deep brain stimulation in swine. *NeuroImage*, 105, 181–188. <https://doi.org/10.1016/j.neuroimage.2014.09.064>
- Rasmussen, S., Greenberg, B., Mindus, P., Friehs, G., & Noren, G. (2000). Neurosurgical approaches to intractable obsessive-compulsive disorder. *CNS Spectrums*, 5(11), 23–34. <https://doi.org/10.1017/S1092852900021891>
- Rauch, S. L., Jenike, M. A., Alpert, N. M., Baer, L., Breiter, H. C., Savage, C. R., & Fischman, A. J. (1994). Regional cerebral blood flow measured during symptom provocation in obsessive-compulsive disorder using oxygen 15—Labeled carbon dioxide and positron emission tomography. *Archives of General Psychiatry*, 51(1), 62–70. <https://doi.org/10.1001/archpsyc.1994.03950010062008>
- Reiss, J. P., Campbell, D. W., Leslie, W. D., Paulus, M. P., Stroman, P. W., Polimeni, J. O., ... Sareen, J. (2005). The role of the striatum in implicit learning: A functional magnetic resonance imaging study. *NeuroReport*, 16(12), 1291–1295. <https://doi.org/10.1097/01.wnr.0000175615.93312.1a>
- Rezaei, A. R., Lozano, A. M., Crawley, A. P., Joy, M. L. G., Davis, K. D., Kwan, C. L., ... Mikulis, D. J. (1999). Thalamic stimulation and functional magnetic resonance imaging: Localization of cortical and subcortical activation with implanted electrodes: Technical note. *Journal of Neurosurgery*, 90(3), 583–590. <https://doi.org/10.3171/jns.1999.90.3.0583>
- Rosenbaum, R., Zimnik, A., Zheng, F., Turner, R. S., Alzheimer, C., Doiron, B., & Rubin, J. E. (2014). Axonal and synaptic failure suppress the transfer of firing rate oscillations, synchrony and information during high frequency deep brain stimulation. *Neurobiology of Disease*, 62, 86–99. <https://doi.org/10.1016/j.nbd.2013.09.006>
- Saikali, S., Meurice, P., Sauleau, P., Eliat, P.-A., Bellaud, P., Randuineau, G., ... Malbert, C.-H. (2010). A three-dimensional digital segmented and deformable brain atlas of the domestic pig. *Journal of Neuroscience Methods*, 192(1), 102–109. <https://doi.org/10.1016/j.jneumeth.2010.07.041>
- Salimpoor, V. N., van den Bosch, I., Kovacevic, N., McIntosh, A. R., Dagher, A., & Zatorre, R. J. (2013). Interactions between the nucleus accumbens and auditory cortices predict music reward value. *Science*, 340(6129), 216–219.
- Schlaepfer, T. E., Cohen, M. X., Frick, C., Kosel, M., Brodesser, D., Axmacher, N., ... Sturm, V. (2008). Deep brain stimulation to reward circuitry alleviates anhedonia in refractory major depression. *Neuropsychopharmacology*, 33(2), 368–377. <https://doi.org/10.1038/sj.npp.1301408>
- Servello, D., Porta, M., Sassi, M., Brambilla, A., & Robertson, M. M. (2008). Deep brain stimulation in 18 patients with severe Gilles de la Tourette syndrome refractory to treatment: The surgery and stimulation. *Journal of Neurology, Neurosurgery & Psychiatry*, 79(2), 136–142. <https://doi.org/10.1136/jnnp.2006.104067>
- Settell, M. L., Testini, P., Cho, S., Lee, J. H., Blaha, C. D., Jo, H. J., Min, H.-K. (2017). Functional circuitry effect of ventral tegmental area deep brain stimulation: Imaging and neurochemical evidence of mesocortical and mesolimbic pathway modulation. *Frontiers in Neuroscience*, 11, 104.
- Swedo, S. E., Rapoport, J. L., Leonard, H., Lenane, M., & Cheslow, D. (1989). Obsessive-compulsive disorder in children and adolescents: Clinical phenomenology of 70 consecutive cases. *Archives of General Psychiatry*, 46(4), 335–341. <https://doi.org/10.1001/archpsyc.1989.01810040041007>
- Van Gompel, J. J., Bower, M. R., Worrell, G. A., Stead, M., Meier, T. R., Goerss, S. J., ... Lee, K. H. (2011). Swine model for translational research of invasive intracranial monitoring. *Epilepsia*, 52(6), e49–e53. <https://doi.org/10.1111/j.1528-1167.2011.03096.x>
- Vincent, J. L., Patel, G. H., Fox, M. D., Snyder, A. Z., Baker, J. T., Van Essen, D. C., ... Raichle, M. E. (2007). Intrinsic functional architecture in the anaesthetized monkey brain. *Nature*, 447(7140), 83. <https://doi.org/10.1038/nature05758>
- Vitek, J. L. (2002). Mechanisms of deep brain stimulation: Excitation or inhibition. *Movement Disorders*, 17(S3), S69–S72.
- Volkow, N. D., Fowler, J. S., Wang, G.-J., Swanson, J. M., & Telang, F. (2007). Dopamine in drug abuse and addiction: Results of imaging studies and treatment implications. *Archives of Neurology*, 64(11), 1575–1579. <https://doi.org/10.1001/archneur.64.11.1575>

How to cite this article: Cho S, Hachmann JT, Balzekas I, et al. Resting-state functional connectivity modulates the BOLD activation induced by nucleus accumbens stimulation in the swine brain. *Brain Behav*. 2019;9:e01431. <https://doi.org/10.1002/brb3.1431>

APPENDIX A**ABBREVIATIONS**

aIC, anterior portion of insular cortex

Am, Amygdala

CD, caudate

daCC, dorsal anterior cingulate cortex

DLPFC, dorsal lateral prefrontal cortex

dpCC, dorsal posterior cingulate cortex

FX, fornix

HP, hippocampus

mdPFC, mid-dorsal lateral prefrontal cortex

mdTH, mediodorsal thalamic nucleus

mPFC, medial prefrontal cortex

NAc, nucleus accumbens

pIC, posterior portion of insular cortex

Pu, putamen

SAC, sensory association cortex

SNc, substantia nigra pars compacta

vaPFC, ventral anterior prefrontal cortex

vaTh, ventral anterior thalamic nucleus